ACS APPLIED MATERIALS & INTERFACES

Forum Article

www.acsami.org

Transport, Phase Reactions, and Hysteresis of Iron Fluoride and Oxyfluoride Conversion Electrode Materials for Lithium Batteries

Jonathan K. Ko,[†] Kamila M. Wiaderek,[‡] Nathalie Pereira,[†] Tiffany L. Kinnibrugh,[‡] Joshua R. Kim,[†] Peter J. Chupas,[‡] Karena W. Chapman,[‡] and Glenn G. Amatucci*,[†]

[†]Energy Storage Research Group, Department of Materials Science and Engineering, Rutgers University, North Brunswick, New Jersey 08902, United States

[‡]X-ray Science Division, Advanced Photon Source, Argonne National Laboratory, Argonne, Illinois 60439, United States

ABSTRACT: Potentiostatic intermittent titration technique (PITT) was applied to FeF_2, FeF_3, and $FeO_{0.67}F_{1.33}$ to gain insight into the transport-related aspects of the conversion reaction by quantitative analysis of Li^+ diffusion and hysteresis. PITT derived diffusion coefficient measurements were benchmarked relative to values extracted by electrochemical impedance spectroscopy (EIS). A reverse-step PITT methodology was used to evaluate true hysteresis by eliminating nucleation induced overpotentials. This method evaluates the minimum potential hysteresis and allowed an accurate representation of the potential required to move conversion reactions forward at $C/1000$ rates in both lithiation and delithiation. The high resolution PITT data were also used to gain further insight into reaction mechanisms involved in the reversible conversion reactions. Physical evidence, based on pair distribution function (PDF) structural analysis, and electrochemical evidence are presented regarding a new step in the reaction during the rutile FeF_2 reconversion reaction.

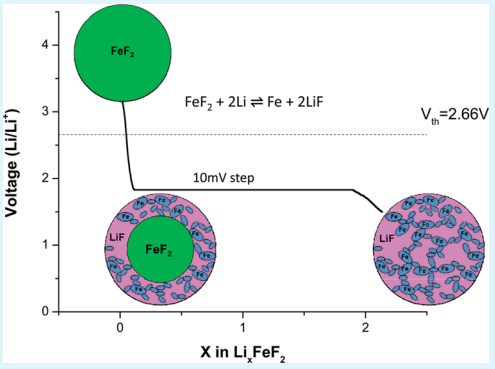

KEYWORDS: *lithium, battery, iron fluoride, transport, hysteresis, PITT*

1. INTRODUCTION

Portable electronics have given rise to improved rechargeable batteries to address demands of power and energy. Current commercial batteries typically contain intercalation cathode materials (e.g., $LiCoO_2$, $LiFePO_4$). Although they provide very good reversibility, they exhibit a limited capacity. At the "true" theoretical capacity, the layered structure only allows one electron transfer per transition metal. In addition, the amount of accessible energy is only a fraction of its true capacity. Conversion materials can have up to four times the typical capacity found in intercalation materials by utilizing all of the metal's redox potential and reducing it to its pure metal state. One of the challenges for conversion materials is the limited mobility of the Li^+ ions to move to the unreacted sites. Electrons are not as limited because a conductive network is formed when the transition metal is reduced allowing an electronic pathway to unreacted sites.[1,2] Fluorides, specifically iron-based, have been a main focus of our group because of their low cost and relatively low toxicity. The high ionic M−F bonds allow higher reduction potentials around 2 V. Herein, we will present data on three transition metal fluorides: FeF_2, FeF_3, and $FeO_{0.67}F_{1.33}$.

When cells are cycled galvanostatically, i.e., under constant current, the voltage profile is a composite of theoretical reaction potential, polarization, and intrinsic hysteresis. Polarization can be reduced dramatically because it is not inherent to a material; in contrast, hysteresis cannot. Intrinsic hysteresis is a common property that is found in all conversion materials and was clearly shown by the Tarascon group[3] for metal oxides and sulfides. Metal fluorides exhibit similar challenges.[4−6] Doe et al, proposed a model for the large intrinsic voltage hysteresis found in FeF_3.[7] Because Fe mobility is slower than Li^+ ions, Li^+ follows a different reaction pathway than what is thermodynamically favorable during the conversion process. As a result, many metastable pathways could be identified through calculations, especially on delithiation with little potential difference.[7] Dissimilarities in reaction mechanism between charge and discharge could account for the presence of intrinsic hysteresis in conversion materials. This is distinct from intrinsic hysteresis postulated for all insertion material systems as discussed by Dreyer and Moskon in their many particle models.[8,9]

Accurate characterization of overpotential and hysteresis is critical to the understanding and optimization of the electrode kinetics, and reaction pathways of conversion materials. In galvanostatic intermittent titration technique (GITT), current is applied in pulses while voltage is monitored. Upon current relaxation, voltage decays to an equilibrium voltage.[10] While this voltage corresponds to a specific lithium concentration in

Special Issue: New Materials and Approaches for Electrochemical Storage

Received: January 24, 2014
Accepted: March 24, 2014
Published: April 8, 2014

the cathode for intercalation materials; this cannot be used for conversion materials since the equilibrium state is split between converted material and unconverted material. More importantly, the relaxation voltage would also be considered the equilibrium potential for both converted and unconverted material to coexist, not for the reaction to proceed. This paper will show that for conversion materials, galvanostatic measurements, although useful for evaluating kinetic polarization, are not as helpful for establishing intrinsic properties and that potentiostat measurements offer a more robust approach.

Potentiostatic intermittent titration technique (PITT) is a related method for studying diffusion and thermodynamics in lithium batteries.[11] Interfacial resistance is negated since the technique involves small increment voltage steps while monitoring the current associated with the reaction to move to equilibrium before moving to the next step. With PITT, one is able to calculate the diffusion coefficient of Li ions, or more specifically, the mobility of the reaction front during the three-phase reaction step. The beginning of every voltage step in PITT establishes a new concentration at the electrode-electrolyte interface. The current response is a result of maintaining the new concentration at the surface while ions diffuse into the electrode until the whole electrode is at equilibrium with the new concentration. We further support this with diffusion coefficients extracted from electrochemical impedance spectroscopy (EIS) measurements. Both diffusion coefficients were measured using the methods found in Huggin's papers.[11,12] Identification of the intrinsic hysteresis potential in conversion materials is not a simple endeavor. Intrinsic hysteresis obtained through PITT can be complicated by the presence of a nucleation overpotential to initiate conversion. To overcome these challenges, we utilized a reverse step potentiostatic intermittent titration technique method in the identification of the reaction potential hysteresis.

2. EXPERIMENTAL SECTION

2.1. Sample Preparation. FeF_2 and FeF_3 were used as received (Advance Research Chemicals) and $FeO_{0.67}F_{1.33}$ was synthesized from a solution of iron metal and fluorosilicic acid and then dried under air as described previously.[13] Carbon nanocomposites of these metal fluorides were prepared by high-energy milling (SPEX 8000). An 85:15 weight ratio between the metal fluoride and activated carbon (Norit A-supra) was placed inside a hardened steel milling cell under He and milled for 30 min. After milling, the composite samples were stored in vials packed under He atmosphere to avoid atmospheric contamination. Electrodes were prepared using the Bellcore method by adding poly(vinylidene fluoride-co-hexafluoropropylene) (Kynar 2801, Elf Atochem), carbon black (Super P, MMM), and propylene carbonate (Aldrich) to the powder in acetone (Aldrich).[14] The slurry was tape cast in a dry room (<1% relative humidity), allowed to dry for 10 min, and rinsed three times in 99.8% anhydrous diethyl ether (Aldrich) to extract the propylene carbonate plasticizer. The electrodes were further dried, under vacuum at 120 °C for 1 h, to remove any residual moisture. Phase purity of materials was confirmed through the use of X-ray diffraction.

2.2. Electrochemical Characterization. Coin cells (2032, Hohsen) were assembled in a He-filled glovebox using Whatman GF/D glass fiber separators saturated with either 1M $LiPF_6$ in ethylene carbonate:dimethyl carbonate (EC:DMC) or 1M $LiBF_4$ in ethyl methyl sulfone (EMS). The metal fluoride nanocomposite electrode was used as the positive electrode while pure lithium metal (FMC) was used as the negative electrode. Batteries were cycled using MacPile (Biologic), VMP 3 (Biologic), and Arbin cyclers for both potentiostat and galvanostat.

Coin cells were cycled in GITT from 4.25 to 1.5 V with 7.5 mA/g (based on weight of active material) pulses for 1 h followed by a 5 h relaxation between pulses. Typical hysteresis is taken from voltage points after relaxation in which polarization is eliminated.

All materials characterized by PITT were cycled from 4.25 V to 1.5 V using 10 mV step size with a current cut-off of 0.4 mA/g ($<C/1000$) of active material. The diffusion coefficient, D was calculated by measuring the linear slope of the $\ln(I)$ vs time (t) at each voltage step. At each voltage step the surface current decays exponentially[11]

$$I(t) = \frac{2z_aFS(C_s - C_o)\tilde{D}}{L}\exp -\frac{\pi^2\tilde{D}}{4L^2}$$

D can then be calculated by taking the linear region in the graph of $\ln(I)$ versus t.

$$\tilde{D} = -\frac{d(\ln(I))}{dt}\frac{4L^2}{\pi^2}$$

Where I is the current of the potential step, t is time within the potential step and L is the diffusion length. In our case we assume our samples are 50 nm spherical particles based on characterization by transmission microscopy.

EIS was measured in the range of potentials between 3.5 V and 1 V using a VMP (Biologic). Cells were discharged for 4 h at 20 mA/g. Before each measurement the cell was allowed to rest for 10 min. The cells were characterized at an amplitude of 10 mV within a frequency range of 200 kHz to 200 μHz. Each spectrum was fitted with a Randle's equivalent circuit (Figure 1). R_0 is the uncompensated ohmic

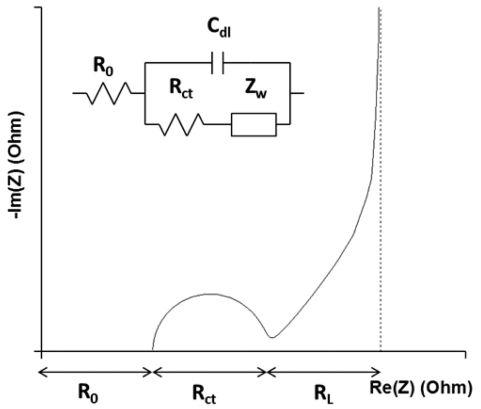

Figure 1. An illustration of Randles circuit.

resistance of the electrolyte and electrode; R_{ct} is the charge-transfer resistance, C_{dl} is the double layer capacitance, Z_w* is the Warburg impedance. Narquisian impedance spectra show a semi-circle at high frequency, which is the combination of R_o and R_{ct}. At very low frequencies, a vertical line in which R reaches its limit is the sum of (R_0 + R_{ct}) and R_L, where R_L is the limiting low-frequency resistance.[10]

The diffusion coefficient can be calculated by the Warburg impedance expressed as

$$Z_W = \sigma(1 - j)\omega^{-1/2}$$

σ is the Warburg coefficient, j is an imaginary unit, and ω is the angular frequency. σ can be found by taking the slope of Re(Z) vs $\omega^{-1/2}$. This can then be used in the equation

$$\sigma = \frac{V_m}{\sqrt{2}\,zFAD_{app}^{1/2}}\frac{dE}{dx}$$

V_m is the molar volume of the cathode, z is the charge transfer between the anode and the cathode, F is Faraday's constant, A is the active surface area of the electrode, and dE/dx the slope of the voltage.

The equation is rearranged to find D

$$D_{app} = \frac{V_m^2}{2z^2F^2A^2\sigma^2}\left(\frac{dE}{dx}\right)^2$$

We followed Ho's[12] assumptions for Fick's diffusion equation, which states that the lithium diffusion into the cathode is a semi-infinite and that during the time period the measurement is taken for, lithium has not penetrated to the end of the cathode. Furthermore, the driving force for diffusion is a gradient in relation to composition and that the electrical field in the electrode can be negated. Lastly, the diffusion coefficient is linearly and independently related to the concentration over the range of the alternating voltage that is applied.[12]

To address the degree of correction required to account for charge transfer considerations, we applied the correction factor approach suggested by Montella[15] utilizing both the EIS and PITT data we have collected.

Diffusion coefficients that were determined within the Cottrellian region can be an underestimation because of kinetic limitations from surface processes and ohmic drop. This can be corrected with the following equation[15]

$$\frac{D_{ap}}{D} = 4\frac{b^2}{\pi^2}$$

D_{ap} is the apparent diffusion coefficient, D is the corrected diffusion coefficient, and is the 1st positive root of the following equation

$$b\tan(b) - \Lambda = 0$$

Λ is the dimensionless parameter. When Λ has a high value ($\log(\Lambda) > 1$), $b = \pi/2$, in which the Cottrellian response is diffusion control and interfacial charge transfer and/or ohmic drop is considered negligible, thus $D_{ap} = D$. The dimensionless parameter is defined as[16]

$$\Lambda = \frac{I(0)\tau_d}{\Delta Q}$$

Where $I(0)$ is the initial current of the step. ΔQ is the total charge transfer during the step and τ_d is

$$\tau_d = \frac{L^2}{D}$$

2.3. Pair Distribution Function (PDF) Analysis. X-ray total scattering data, suitable for PDF analysis, were collected at the beamline 11-ID-B at the Advanced Photon Source, Argonne National Laboratory, for electrodes recovered from selected states of lithiation and delithiation. Electrode samples were prepared as described above, cycled galvanostatically at 60 °C at 50 mA/g (with respect to the nanocomposite) for FeF_2 and $Fe_{0.67}F_{1.33}$ and at 7.5 mA/g for FeF_3, removed from the coin cell, transferred to an inert X-ray sample environment and mounted on the instrument perpendicular the beam. High-energy X-rays (λ = 0.2114 Å) were combined with a large area detector (Perkin-Elmer amorphous-silicon) to collect data to high values of momentum transfer with exposure times of 5 min.[17,18] The scattering images were reduced to one-dimensional data within fit2d.[19,20] The data were corrected for background scattering, Compton scattering and detector effects within PDFgetX2 and Fourier transformed to Q_{max} = 19 Å^{-1} to obtain the PDF, $G(r)$.[21] Structural models were refined against the PDF data within PDFgui.[22]

Comprehensive structural phase analyses have been performed for a series of samples recovered following the 1st, 2nd, 10th, and 20th lithation and delithation processes. The detailed results of these analyses will be reported elsewhere. Here, we focus on the structural models refined for the rock salt LiF component(s).

3. RESULTS

3.1. GITT. FeF_2−C nanocomposites were pulsed in GITT mode during lithiation and delithiation for 1 h at 7.5 mA/g with a 5 h relaxation between pulses at 25 °C shown in Figure 2. The overpotential before the ∼1.8 V plateau corresponds to nucleation and growth of the 2LiF + Fe product of the conversion reaction.[23] The average OCV (Open Circuit Voltage) upon lithiation is ∼2.2 V from x = 0.25−1.5. On delithiation, the average OCV was 2.7 V from x = 1.75−1.

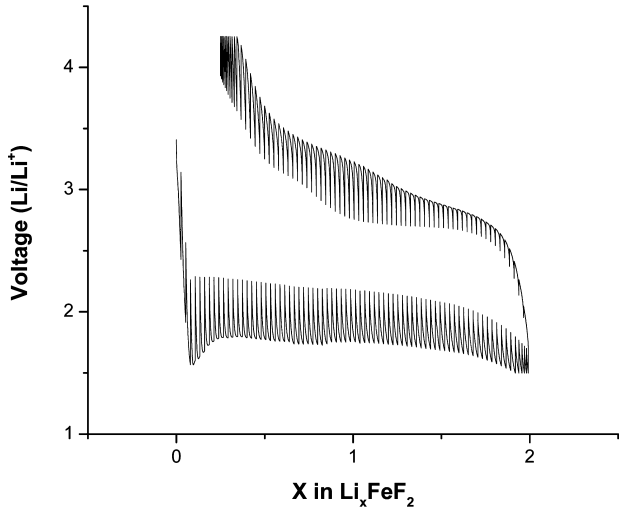

Figure 2. GITT of FeF_2−C nanocomposites, 7.5 mAh/g with 1 h cutoff follow by 5 h open circuit relaxation at 25 °C.

Traditionally, post pulse OCV such as these have been presented as an indication of the true hysteresis of the reversible conversion reactions. Upon closer inspection, however, one can see (FeF_2, x = 0.25, in Figure 3) that the

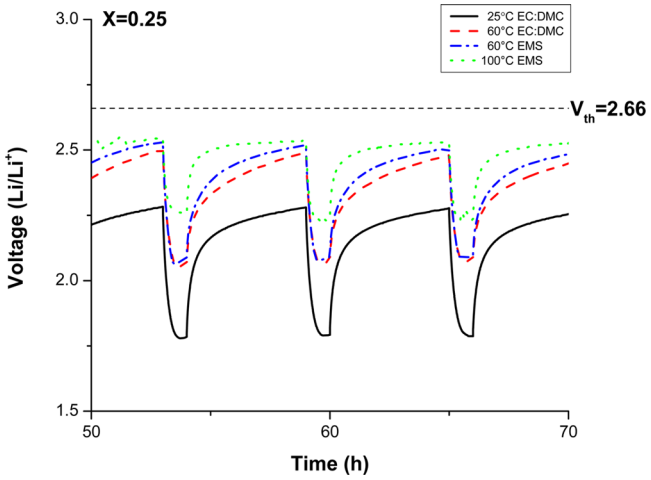

Figure 3. GITT of FeF_2−C nanocomposites during lithiation at various temperatures, 7.5 mAh/g with 1 h cutoff follow by 5 h open circuit. Shown at x = 0.25 in Li_xFeF_2. 1 M $LiPF_6$ in EC:DMC was used at 25 and 60 °C while 1 M $LiBF_4$ in EMS was used at 60 and 100 °C.

voltage during relaxation has not truly relaxed to an equilibrium value. Compared to the theoretical value (V_{th} = 2.66 V), the relaxation voltage after 5 h is about 2.28 V. The true relaxation voltage can be approached by allowing a longer relaxation time or by increasing the temperature which in turn will increase the kinetics and thus drive the reaction closer to equilibrium potential. EMS was used for electrochemistry at temperatures 60 °C and greater because of the solvent stability up to 220 °C.[24] The effect of temperature on the voltage polarization and hysteresis is also seen in Figure 3. The polarization induced voltage during the lithiation pulse is systematically decreased (from 2.28 to 2.53 V) with an increase in temperature (from 25 to 100 °C). More importantly, from the context of this paper, the kinetics of the relaxation was much improved revealing that the room temperature relaxation values established through

GITT at 25 °C are far from equilibrium. Even though the response at 100 °C is much faster, no equilibrium value have been reached.

To gain a greater insight into the true equilibrium value, we fitted the lithiation and delithiation profiles of the relaxation for each temperature. Results show that the relaxation curves from lithiation and delithiation require extraordinarily long times to access a near equilibrium value. Extension of the fits for approximately 10 days shown in Figure 4 reveals that, within

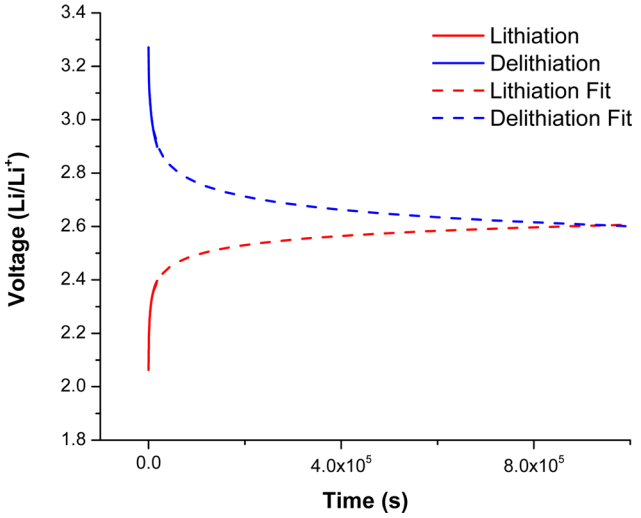

Figure 4. Fit of the relaxation curve of FeF_2−C nanocomposites GITT at 60 °C at x = 1 in Li_xFeF_2. Electrolyte was $LiBF_4$ in EMS.

error of the extensive fit, relaxation potentials approach an equilibrium value near 2.6 V and no intrinsic hysteresis can be determined using the relaxation technique. This should be expected, as the relaxed value of a true conversion reaction during GITT should not be indicative of any hysteresis when comparing the delithiation and lithiation reaction. However, the "on" pulse in GITT gives excellent insight into overpotential + hysteresis characteristics. Indeed, the conversion reaction may require a minimum potential to activate a reaction pathway even at near equilibrium rates. As such, well controlled PITT may represent a better path of understanding as the potential is controlled and the limiting potential required to induce the onset of the reaction can be identified.

3.2. PITT. Figure 5 shows the voltage profile of FeF_2−C nanocomposite electrode characterized utilizing a very slow rate PITT discharge where a typical lithiation reaction requires 2 months. The voltage steps down in small 10 mV steps and does not continue to the next step until the current decays to <0.4 mA/g (approximately C/1000). Commencing with an initial OCV of 3.39 V, the discharge proceeds without any significant increase in the current until 1.84 V. At this potential, the entire $FeF_2 \rightarrow 2LiF + Fe$ reaction proceeds to near completion in a single 10 mV step.[1,4] In sharp contrast to this lithiation behavior, even at the very low C/1000 rate, the delithiation proceeds in a more solid solution like manner over many steps. These data are strong evidence that the delithiation reaction proceeds in a mechanism that is unlike the lithiation reaction. Before making such a conclusion, the second lithiation was investigated because of the considerable polarization observed in the first lithation for most conversion materials. The second lithiation reveals a small 3 V reaction shown in Figure 6. This is attributed to a small degree of Fe^{3+} formation as a result of Fe^{2+}

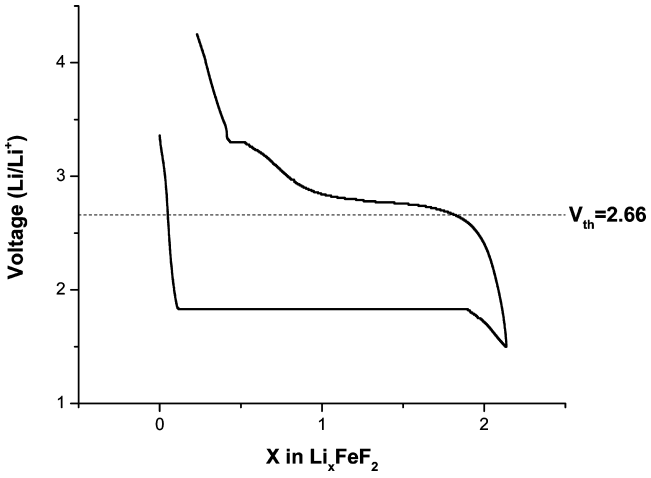

Figure 5. First PITT cycle of FeF_2−C nanocomposites, 10 mV step 0.4 mA/g current cutoff at 25 °C.

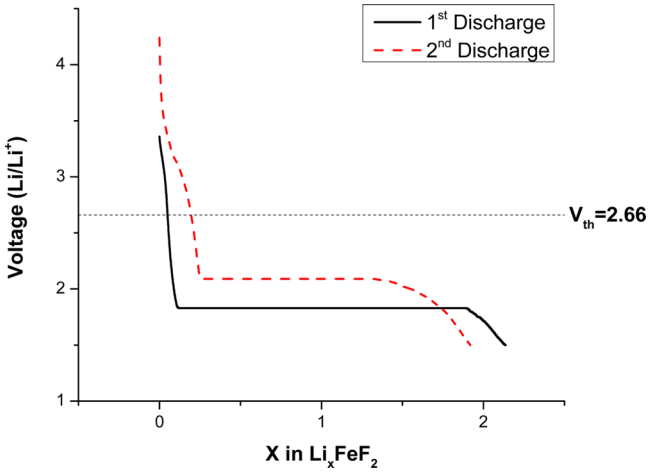

Figure 6. First and second PITT discharge of FeF_2−C nancomposites, 10 mV step 0.4 mA/g current cutoff at 25 °C.

loss through dissolution.[1] Again, the conversion step is seen to proceed in a single-step reaction that occurs entirely within a 10 mV step. However, the onset potential of this step at 2.09 V is significantly higher than the first lithiation. This shift in conversion potential can be attributed to the significantly finer nanostructure of the reformed FeF_2 particles undergoing conversion, typically 10 nm vs 20 nm. As such, a smaller nucleation overpotential may be required.

Iron(III) fluoride (FeF_3) was investigated as a contrasting case of conversion. Figure 7 is the voltage profile of FeF_3−C nanocomposite electrode under similar 10 mV step PITT conditions. The PITT lithiation commenced at an OCV of 3.63 V. A lithium insertion reaction commences at 3.36 V. There the lithium inserts in a two-phase reaction as evidenced by the quasi plateau of potential steps. This proceeds to approximately x = 0.242 in Li_xFeF_3. This is consistent with the two-phase reaction[4] leading to a defective rutile like structure of an approximate composition of $Li_{0.5}FeF_3$.[7,23] Further lithiation forms a metastable solid solution of $LiFeF_3$. At 1.89 V, the conversion process of $LiFeF_3 \rightarrow 3LiF + Fe$ proceeds in a single 10 mV step, although a bit short of full completion. This is remarkably similar to the 1.84 V onset potential of conversion observed for the FeF_2 material. This is also consistent with previously reported data where the plateau represents the

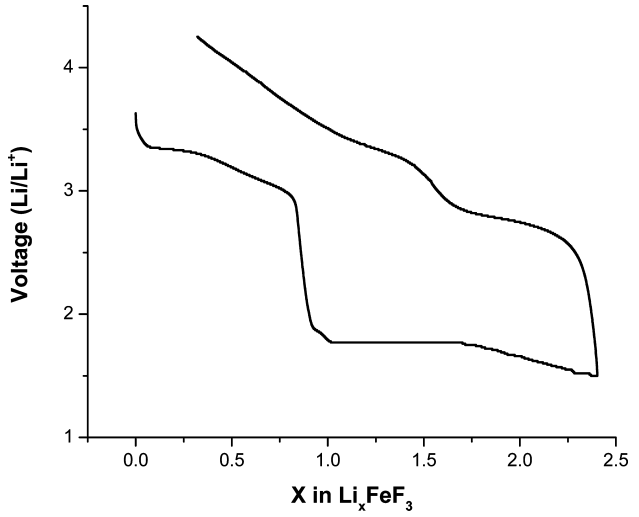

Figure 7. First PITT cycle of FeF_3–C nancomposites, 10 mV step 0.4 mA/g current cutoff at 25 °C.

reduction of Fe^{2+} to Fe^{0}.[4,25] As with FeF_2, the delithiation occurs over a large multitude of small 10 mV steps, far from the behavior one would expect in a "reconversion" reaction. As an aggregate of small steps, this delithiation proceeds with two general plateau-like areas in contrast to FeF_2. This suggests origins in the $Fe^{o} \rightarrow Fe^{2+}$ and $Fe^{2+} \rightarrow Fe^{3+}$ redox reactions. On the second lithiation, there is no indication of a $Li_{0.5}FeF_3$ phase formation via plateau formation at the higher voltage regions (Figure 8). This is consistent with the reported spectroscopy[4,23]

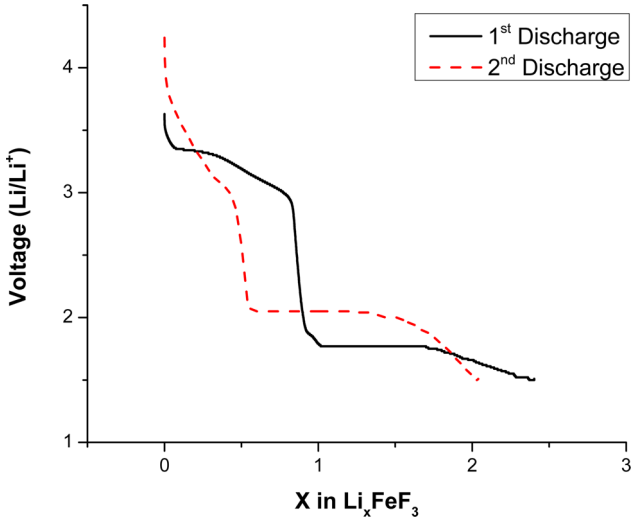

Figure 8. First and second PITT discharge of FeF_3–C nanocomposites, 10 mV step 0.4 mA/g current cutoff at 25 °C.

which indicates that the reconverted FeF_3 is more rutile like in nature thus not requiring the structural transformation observed in the first lithiation of the ReO_3-like FeF_3 original phase. FeF_3 experiences a higher onset potential for conversion during the second cycle associated with the smaller crystallite size formed following reconversion.

$FeO_{0.67}F_{1.33}$ was investigated as a hybrid between FeF_2 and FeF_3 in which the Fe^{3+} exists in a FeF_2 rutile structure instead of the ReO_3 structured FeF_3. $FeO_{0.67}F_{1.33}$ has a starting OCV of 3.54 V. Upon lithiation under PITT protocol, $FeO_{0.67}F_{1.33}$ proceeds with solid solution like behavior as lithium is inserted into the structure forming a lithiated rocksalt type phase ($Li_{0.7}FeO_{0.7}F_{1.3}$). This seems contrary to expected behavior but will be discussed in more detail in the discussion. The reaction potential is consistent with lithium insertion to reduce $Fe^{3+} \rightarrow Fe^{2+}$.[13] This proceeds until $x = 0.516$ in $Li_xFeO_{0.67}F_{1.33}$ where the onset of the "conversion" reaction occurs at 2.1 V, significantly higher than the onset potential of either FeF_2 or FeF_3 during the first lithiation. As opposed to the conversion reaction proceeding to completion in one single 10 mV step for the conversion reaction of FeF_2 or FeF_3 in the first or second lithiation, numerous potentials are required (Figure 9) for the

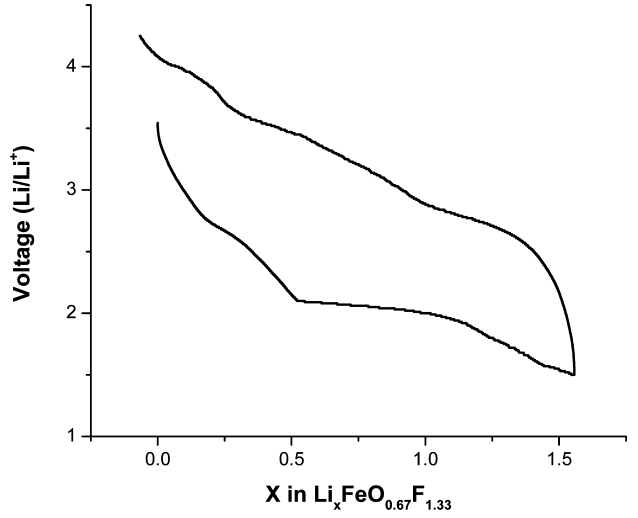

Figure 9. First PITT cycle of $FeO_{0.67}F_{1.33}$–C nanocomposites, 10 mV step 0.4 mA/g current cutoff at 25 °C.

conversion reaction of $FeO_{0.67}F_{1.33}$ to fully proceed. As such, the $FeO_{0.67}F_{1.33}$ material displays a distinctly unique conversion behavior during lithiation. The higher onset potential of the conversion can be explained by spectroscopic evidence suggesting that the rocksalt phase and possibly the Fe metal is already present in the latter part of the lithium insertion reaction which occurs at higher potentials than the conversion reaction.[26,27] As such, these phases are already nucleated before the conversion step. The conversion reaction, consisting of many small plateaus, can be attributed to compositional changes with new phases forming from conversion or from the gradient of oxygen in the composition.[28] This will be discussed in further detail below within the discussion.

The delithiation reaction of $FeO_{0.67}F_{1.33}$ is very similar to that of FeF_3 and FeF_2 in that it is composed of hundreds of small 10 mV regions clearly showing the potential is changing systematically with compositional change. It is similar to the delithiation of FeF_3 in that it has two regions that can be attributed to the oxidation of the Fe. Indeed, the approximate location of these segments are consistent with $Fe^{0} \rightarrow Fe^{2+}$ and $Fe^{2+} \rightarrow Fe^{3+}$ oxidation regions as shown by in-situ Mossbauer.[29] The second lithiation shows a higher voltage region of quite different potential dependence than the first lithiation. This may be in part attributed to small amounts of rocksalt phase known to be present during the delithiation and the nanostructure is near amorphous therefore leading to insertion with minimal reconstruction.[26] In sharp contrast to the FeF_2 and FeF_3, $FeO_{0.67}F_{1.33}$ shows very little change in the onset potential of the second cycle conversion relative to the first lithiation. This gives support to the fact that the preconversion

structure is highly favorable for the conversion reaction to proceed in the case of $FeO_{0.67}F_{1.33}$. As from Figure 10,

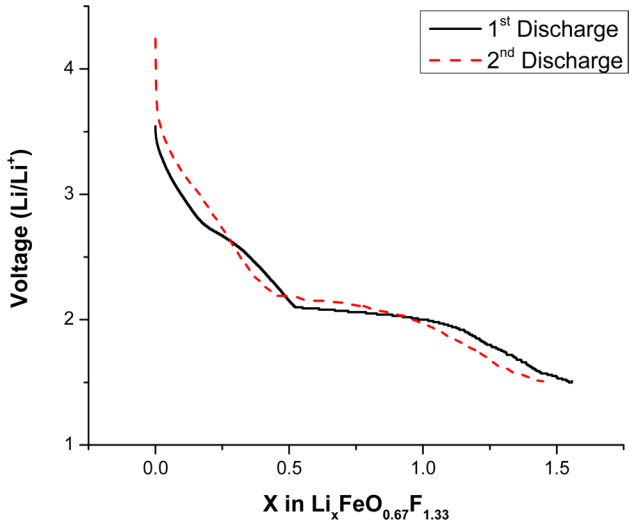

Figure 10. First and second PITT discharge of $FeO_{0.67}F_{1.33}$—C nanocomposites, 10 mV step 0.4 mA/g current cutoff at 25 °C.

$FeO_{0.67}F_{1.33}$ maintains the same voltage profile during the second lithiation as with the first with the exception of a higher conversion voltage at 2.19 V from the reduced particle size.

3.3. Diffusion Coefficients. Diffusion coefficients were extracted from the PITT data. As a benchmark, EIS was also used to calculate the diffusion coefficients. It is certainly well-known that PITT-derived diffusion coefficient in multiphase reactions is not a direct representation of D_{Li} but rather an effective diffusion coefficient or pseudo diffusivity coefficient which reflects the interface movement and the diffusion of other species. PITT has been demonstrated as an acceptable approach for the study of interface mobility in a number of multiphase electrode reactions[30−37] and against it if not corrected for charge transfer effects,[15,16,38] as discussed below. Some theorize the small region of Cottrellian behavior observed within the PITT response of multiphase reactions is due to a localized range of solid solutions reactions occurring at a very small length scale where the interface moves forward, thus fundamentally dependent on diffusion processes. Regardless of the true nature of the correlation, the diffusion coefficient derived by PITT in multiphase behavior has been seen to be remarkably close to true time scales of the reactions and similar (within to order of magnitude) to corrected methodologies in many published accounts. We only utilize the Cottrellian-like linear behavior region within the non-Cottrellian current evolution, which is typical of multiphase reactions. Indeed, the results from PITT contain a collection of transport phenomena including the bulk diffusion of lithium and other species which contribute to the boundary diffusion as described above and also charge transfer. The latter is the latest focus of correction as it impacts the interpretation of the voltage step intrinsic to the PITT technique. In certain transport scenarios, interface resistance could lead to a source of serious underestimation of the bulk diffusion coefficient.[15] The basis for this rests in an uncorrected charge transfer and solution resistance, which effects both the short-term and long-term current decay response and thus the calculation of the diffusion coefficient. This can be corrected by the use of the dimensionless parameter (Λ), where if there is little charge transfer resistance relative to diffusion, large Λ, no correction is needed, where the opposite is enacted for contrasting situations. This theory was also used as a correction factor by Dell'Era et al.[33] and others. Alternative methodologies have been developed by Vorotyntsev et al.,[16] Li et al.[38] utilizing a Biot number correction and others. Following the approach by Montella detailed in the experimental section, our calculations revealed large Λ for all three model materials. For example, the dimensionless parameter was found to be 84 for FeF_2, which indicate a bulk diffusion controlled process and no correction required.

Figure 11 is a comparison of the voltage profiles observed during the intermittent EIS and PITT. Both have similar voltage profiles. The only difference arises from the x value which is a direct result of the faster discharge rate on the cells used for EIS. The calculated diffusion coefficients from both PITT and EIS are shown in Table 1. The values are mostly similar, being within at most 1 order of magnitude to each other. It is possible that this discrepancy is due to the fact that the EIS measurements were taken when the samples were not

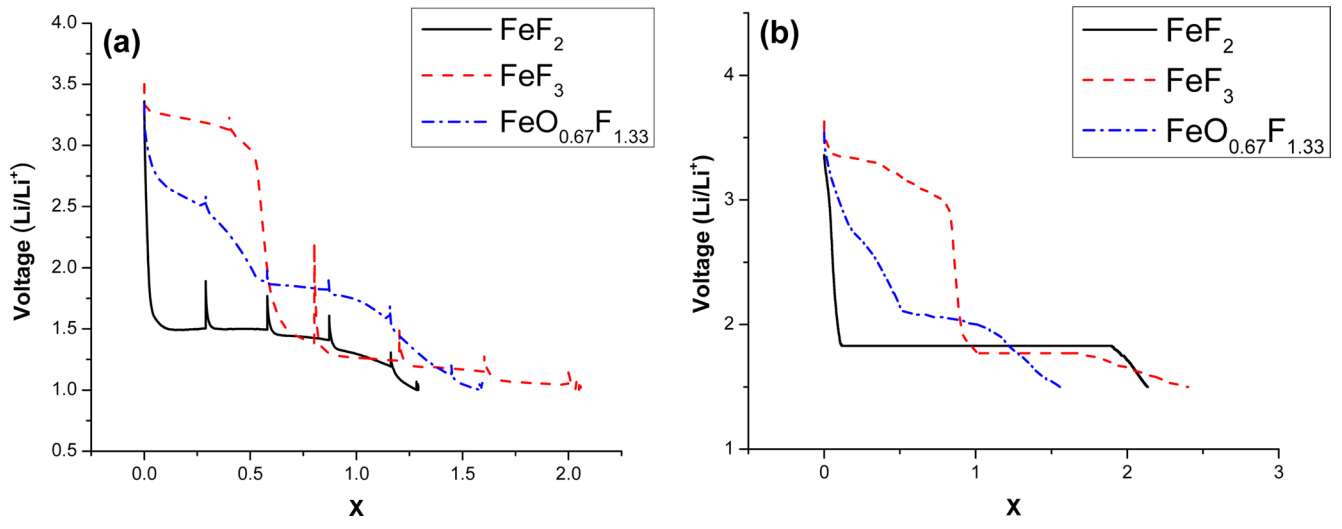

Figure 11. Voltage profile of x in Li_xFeF_3, Li_xFeF_2, and $Li_xFeO_{0.67}F_{1.33}$ taken from: (a) EIS and (b) PITT analysis.

Table 1. Diffusion Coefficient of FeF_2, FeF_3, $FeO_{0.67}F_{1.33}$ Extracted from PITT and EIS Characterization

region	PITT diffusion coefficient (cm^2/s)	EIS diffusion coefficient (cm^2/s)
FeF_2-C		
conversion	4.04×10^{-18}	1.01×10^{-19}
FeF_3-C		
insertion	2.32×10^{-17}	3.21×10^{-18}
conversion	1.71×10^{-18}	1.66×10^{-18}
$FeO_{0.67}F_{1.33}$-C		
insertion	9.35×10^{-17}	1.99×10^{-17}
conversion	3.19×10^{-18}	8.89×10^{-19}

in full equilibrium as impedance was taken after a constant current discharge.

Comparing the PITT observed results for FeF_2 and FeF_3; FeF_2 had a diffusion rate of 4.04×10^{-18} cm^2/s, FeF_3 had a rate of 1.71×10^{-18}. It is understandable that FeF_2 is faster as it can demonstrate higher *C*-rates as a result of less LiF molarity to diffuse through in the converted compound. $FeO_{0.67}F_{1.33}$ diffusion rate is 3.19×10^{-18} cm^2/s, which is close to that of FeF_2 although $FeO_{0.67}F_{1.33}$ can demonstrate a faster *C*-rate, which seems to suggest that the limitation is not due to lithium diffusion and that the large series of multiphasic reactions seen from PITT is benefiting overall reaction kinetics. In general, all coefficients are quite low, thus supporting the requirement for nanomaterials and nanocomposites to enable practical rate reactions to proceed.

3.4. Reverse Step PITT. In PITT, voltage is controlled while the current is monitored to eliminate the polarization effect seen in galvanostatic mode. The goal is to identify the absolute minimum potential it takes for the reaction to proceed forward in order to accurately define "hysteresis" vs. kinetically induced polarization. However, as shown above, in some of the conversion materials, there is a significant amount of overpotential that must be addressed in order to initiate the conversion process. In PITT, after the initiation of the reaction, the reaction then proceeds at a voltage that may be in considerable excess of the subsequent true potential needed to carry out the reaction. As such, it would be fruitless to utilize this potential to calculate intrinsic hysteresis between the lithiation and delitiation reactions.

It has been noted that FeF_2 and FeF_3 have an overpotential that is associated with nucleation and growth.[23] To separate the hysteresis from this initial "nucleation-like" activation overpotential, we employed reverse step PITT. In reverse step PITT, we commence with the same conditions as normal PITT, i.e., lowering the voltage in (10 mV/0.4 mA/g current cutoff) steps until a certain predefined capacity is reached. At that point (V_1), we reverse the 10 mV voltage step direction and continue until the cell is unable to discharge 3 mAh/g within 18 h in a single step. Generally, the current at this point is ~*C*/3000 and is labeled as "V_3" in Figure 12. V_2 is noted as the point in which the current has dropped to 0.4 mA/g (*C*/1000). Afterwards, PITT in the original direction is resumed. By reversing the step direction, we eliminate lithiation driven by overpotential required by the initial nucleation. Indeed, lithiation still occurs but at a much slower rate for every 10 mV step in the reverse direction. Eventually, conversion lithiation reaction cannot proceed as the potential is too high. The voltage found at "V_3" is determined to be the true reaction activating potential. Hysteresis is found by taking the difference

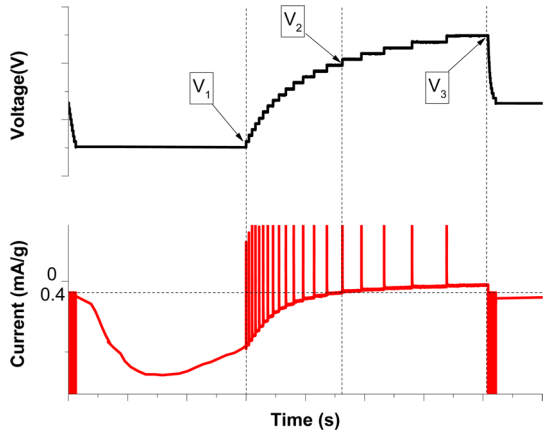

Figure 12. Typical Reverse step PITT voltage profile during lithiation. V_1, V_2, and V_3 are voltages at: initiation of reverse step PITT, the current decay to 0.4 mA/g, and the point where the cell is unable to discharge 3 mAh/g within 18 h in a single step.

of "V_3" found in the lithiation and delithation direction at similar lithium contents (Li_x). In our study, cells were lithiated 10 mV steps with a 0.4 mA/g (<*C*/1000) current cut-off until the following capacities are reached: 100, 198, 200, 290, 450, and 480 mAh/g of active material. The true reaction hysteresis was determined by finding the true activating voltage in lithation and delithiation at the same lithium concentration.

The voltage points collected from reverse step PITT for FeF_2, FeF_3 and $FeO_{0.67}F_{1.33}$ are shown in Table 2. The reaction hysteresis was extracted by finding the difference in voltages at V_3 found in both lithiation and delithiation for each specific capacity. This is shown for each material in Table 3. Reverse step PITT was performed at three points in the two-phase lithiation reaction for FeF_2 cycle (100, 200, 450). Voltage profiles can be seen in Figure 13. Results indicate that the FeF_2 conversion reaction was initiated at ~1.85 V and continued until it reach the targeted capacities. Voltage steps were reversed at the targeted capacity and the reaction persisted until the potential was raise to ~2.05 V, at which the cell is no longer able to maintain conversion. This large 200 mV difference is consistent with the "nucleation − like" overpotential shown in Figure 2. In addition, all cells exhibit a higher potential for the reaction to move forward when resuming normal direction PITT reaction as continued reaction proceeds from the prenucleated conversion front. In sharp contrast, the points taken on delithiation revealed that FeF_2 was able to maintain reconversion for only a very short period after reversing the step potential downward. The potential difference ($V_3 - V_1$) in delithiation is very much lower than on lithiation (50 mV as opposed to 200 mV). This is mainly from the lack of a "nucleation-like" overpotential as seen in lithiation. Because the reaction pathway is different on delithiation, the voltage "V_3" will differ significantly depending on *x* in Li_xFeF_2.

The reaction hysteresis taken at 200 mAh/g (0.7 mol Li) is 1.28 V, whereas the hysteresis found at 100 mAh/g (0.35 mol Li) is 1.75 V as shown in Table 3. Compared to the thermodynamically derived theoretical FeF_2 conversion potential of 2.66 V for FeF_2, the V_3 value on delithiation is much closer (50 mV) to the theoretical potential than on lithiation (830 mV) at the 450 mAh/g data point. In contrast, the values for 100 mAh/g show that the difference for delithiation is larger than for lithiation (1.16 V vs. 0.59 V).

Table 2. Reverse Step PITT of FeF_2, FeF_3, $FeO_{0.67}F_{1.33}$ at Various Capacities[a]

	capacity (mAh/g)	X	V_1 (V)	V_2 (V)	V_3 (V)	$V_3 - V_1$ (V)
			FeF_2			
lithiation						
	25	0.09	1.86	2.02	2.07	0.21
	25	0.09	1.86	2.04	2.06	0.20
	100	0.35	1.89	2.00	2.07	0.18
	100	0.35	1.89	2.00	2.06	0.17
	200	0.70	1.85	2.00	2.05	0.2
	200	0.70	1.93	2.03	2.11	0.18
	450	1.58	1.82	1.94	1.99	0.16
2nd lithiation	100	0.35	2.18	2.27	2.33	0.15
EC:DMC 60 °C	200	0.70	2.28	2.43	2.46	0.18
EC:DMC 60 °C	200	0.70	2.07	2.23	2.29	0.22
EMS 60 °C	200	0.70	2.13	2.26	2.29	0.16
EMS 100 °C	200	0.70	2.28	2.42	2.46	0.18
delithiation						
	450	1.58	2.73	2.72	2.71	0.02
	450	1.58	2.73	2.72	2.70	0.03
	200	0.70	3.38	3.37	3.33	0.05
	100	0.35	3.86	3.85	3.82	0.04
			FeF_3			
lithiation						
	100	0.42	3.22	3.23	3.26	0.04
	100	0.42	3.22	3.22	3.26	0.04
	290	1.22	1.73	1.87	2.03	0.30
	480	2.02	1.73	1.76	1.91	0.18
delithiation						
	290	1.22	3.36	3.35	3.29	0.07
			$FeO_{0.67}F_{1.33}$			
lithiation						
	100	0.34	2.79	2.80	2.80	0.01
	198	0.68	2.23	2.25	2.25	0.02
	198	0.68	2.09	2.10	2.12	0.03
	290	0.99	2.03	2.06	2.08	0.05
delithiation						
	290	0.99	2.78	2.77	2.76	0.02
	290	0.99	2.79	2.79	2.76	0.03
	290	0.99	2.68	2.67	2.64	0.04
	198	0.68	3.09	3.08	3.06	0.03
	198	0.68	3.15	3.14	3.12	0.03
	198	0.68	3.01	3.00	2.98	0.03

[a]Duplicate cells are reported to show reproducibility.

Table 3. Table of Calculated Reaction Hysteresis

capacity (mAh/g)	lithiation V_3 (V)	delithiation V_3 (V)	(ΔV) reaction hysteresis (V)
		FeF_2	
100	2.07	3.82	1.75
200	2.05	3.33	1.28
450	1.99	2.71	0.72
		FeF_3	
290	2.02	3.29	1.27
		$FeO_{0.67}F_{1.33}$	
198	2.12	2.98	0.86
290	2.08	2.64	0.56

Referring to Table 2, FeF_3 was able to maintain lithiation by conversion reaction when the voltage was reversed and increased by 300 mV in its conversion region (290 mAh/g). In contrast, the voltage only stepped up 40 mV before the lithiation reaction stopped when reverse step PITT was performed during the initial lithium insertion, nonconversion, region at 100 mAh/g. Similar to FeF_2, the "nucleation − like" overpotential is what contributes to the large potential difference seen in the conversion region.[25] Also FeF_3 exhibits a higher potential (1.83 V) at 380 mAh/g when resuming downward PITT for lithiation than the potential observed at the start of reverse step PITT (1.73 V) as shown in Figure 14. Reverse step PITT did not have much effect on delithiation, at 290 mAh/g FeF_3 was only able to maintain reconversion for a 70 mV decrease in voltage. From Table 3 the reaction hysteresis at 290 mAh/g is 1.27 V.

In $FeO_{0.67}F_{1.33}$, reverse step PITT was performed at 198 mAh/g in the insertion region and 290 mAh/g in the conversion region. Voltage profiles of both are shown in Figure 15. In the insertion region, the $FeO_{0.67}F_{1.33}$ reaction quickly ceases after the potential was increased by only 20 mV. For the conversion region, unlike FeF_2 or FeF_3, the voltage increased only 50 mV before the reaction ceased, in sharp contrast to the large values of FeF_2 and FeF_3. This is also in agreement with its voltage profile as $FeO_{0.67}F_{1.33}$ has no overpotential as seen in FeF_2 and FeF_3.[13] On delithiation, both measurements taken at 198 and 290 mAh/g reveal that $FeO_{0.67}F_{1.33}$ was only able to maintain reconversion with a small difference in potential (<50 mV difference). From Table 3, the conversion reaction hysteresis found at 290 mAh/g ($x = 0.797$) is 0.56 V much lower than the hysteresis values observed for FeF_2 and FeF_3 conversion.

4. DISCUSSION

4.1. PITT and Reaction Mechanisms. Insight regarding the progression of phases and their respective electrochemical potential can be extracted by thermodynamics and Gibb's phase rule as presented in early work by Huggins and others.[39−41] The phase rule, $F = C - P + 2$, where F is defined as the degrees of freedom, C the number of components, and P the number of phases, can be reduced to $F = C - P$ under conditions of constant temperature and pressure. In the case of single phase topotactic insertion such as Li_xTiS_2, $C = 2$ (Li^+ guest and TiS_2 host), $P = 1$, and thus $F = 1$. The electrochemical potential and phase composition will change as a function of lithiation. If two phases form such as in the $Li_4Ti_5O_{12}/Li_7Ti_5O_{12}$ reaction, $F = 0$, the potential and phase composition, will remain the same as a function of lithiation. Conversion reactions are interesting as they seemingly represent a case of $C = 2$ (Li and FeF_2) and $P = 3$ (FeF_2/Fe/LiF), resulting in $F = -1$. However, in this case, it is apparent that there are two moving species, the Li^+ and either Fe^{2+} or F^- to allow the conversion reaction to proceed. This represents a case of $C = 3$ (Li, Fe, F) and $P = 3$ resulting in F=0 and a constant potential as a function of lithiation. Such a situation is undoubtedly consistent with the experimental results of this paper with the near complete conversion of FeF_2 and $LiFeF_3$ within a span of 10−20 mV, even when corrected for overpotential.

The reaction mechanism becomes increasingly complex as we move to the delithiation reaction of these conversion fluorides. Examination of the high resolution PITT with C/1000 current cutoff clearly shows that for FeF_2 and FeF_3, the

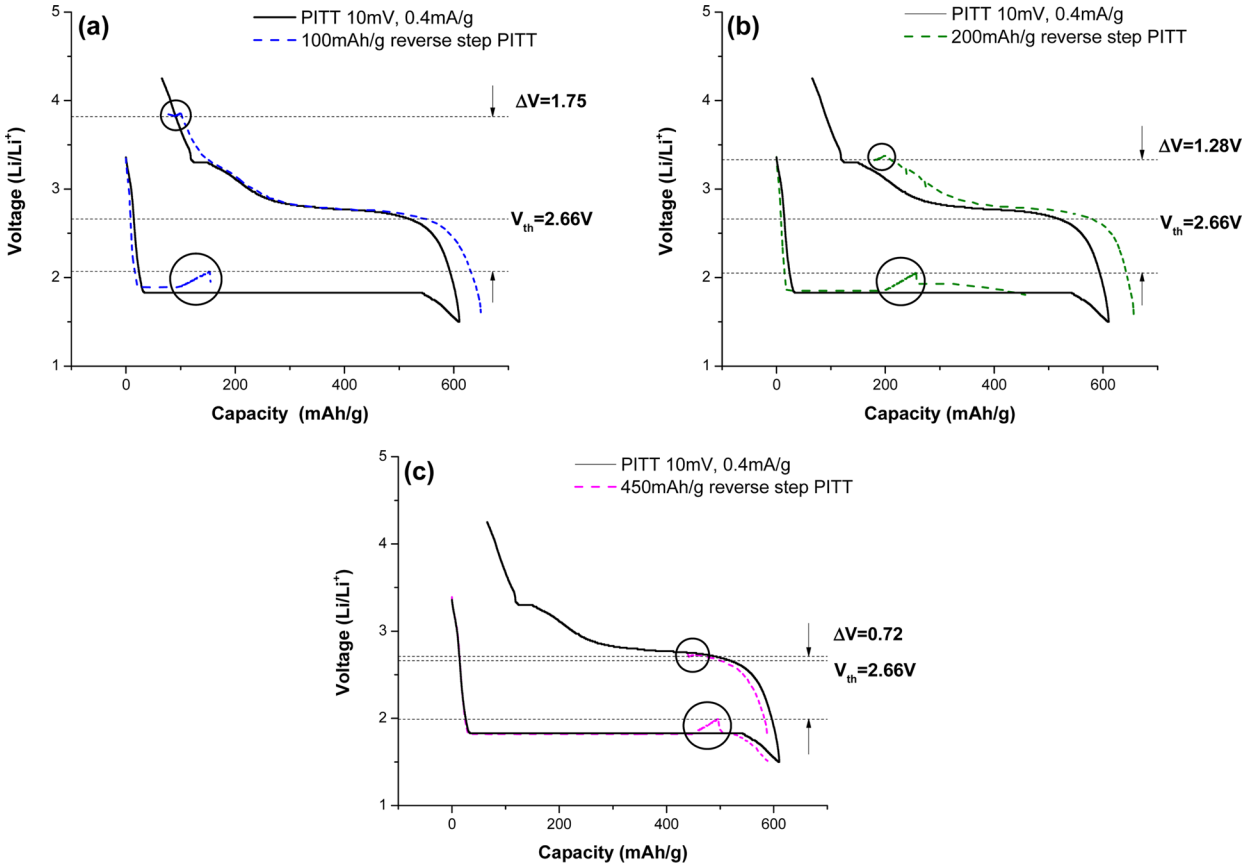

Figure 13. Reverse step PITT of FeF_2 with its normal PITT overlay for capacities, the reverse step PITT portion are indicated with circle: (a) 100 mAh/g (x = 0.35), (b) 200 mAh/g (x = 0.70), (c) 450 mAh/g (x = 1.58).

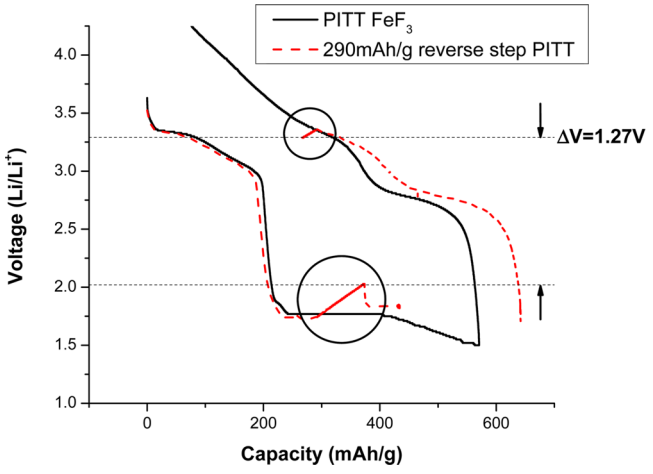

Figure 14. Reverse step PITT of FeF_3 with its normal PITT overlay for 290 mAh/g (x = 1.22) in the conversion region, the reverse step PITT portion is indicated with circle.

delithiation reaction requires a systematic increase in the potential with small degrees of constant potential, most within a $\Delta x \ll 0.2$, representing multiphase equilibrium reactions. This is much more apparent in the case of FeF_3 where the Δx is $\ll 0.1$ for the entire delithiation reaction. Although small, the constant potential vs composition plateaus are not insignificant. This suggests small compositional windows of phase equilibrium. For FeF_2, one could imagine a delithiation reaction scenario following 2 vs. the overall reaction of (1). As a function of delithiation, a multiphase reaction results in an increasing, but not complete degree of delithiation. This phase could be envisioned as Fe^{2+} inserted into the rocksalt LiF, after which a rutile phase is formed upon reaching a Fe saturation threshold. Although the transformation back to rutile FeF_2 has been experimentally confirmed in numerous studies,[1,2,4] we explored whether there was evidence of a rocksalt solid solution precursor to such a transformation.

$$2LiF + Fe \rightarrow FeF_2 + 2Li^+ \quad (1)$$

$$2LiF + Fe \rightarrow (1 - x)Fe + Fe_xLi_{2-2x}F_2 + 2xLi^+ \quad (2)$$

PDF was utilized to explore the delithiation reaction in detail. At the end of FeF_2 lithation processes, the expected rocksalt-type LiF phase is evident in the PDF data, with a refined lattice parameter of ca. 4.035 Å as shown in Figure 16 in close correspondence with the literature values (a = 4.03 Å). Although rocksalt-type LiF is expected to be completely consumed by the delithation reaction resulting in the reformation of rutile FeF_2, delithiation was found to be incomplete as evidenced by a small amount of residual metallic Fe and rocksalt phase. The rocksalt phase observed upon delithiation has a significantly (~1.4%) larger lattice parameter (a = 4.09 Å) than for lithiation (or pristine LiF). Preliminary in situ data which will be reported elsewhere indicates Fe insertion into LiF precedes the formation of rutile FeF_2. The LiF lattice parameter grows progressively in the initial stages of delithiation suggesting a Fe-LiF with progressively increasing Fe content. Fe-LiF can be observed without the presence of rutile but not rutile without Fe-LiF. The increase in the LiF rocksalt lattice dimension can be attributed only to a change in

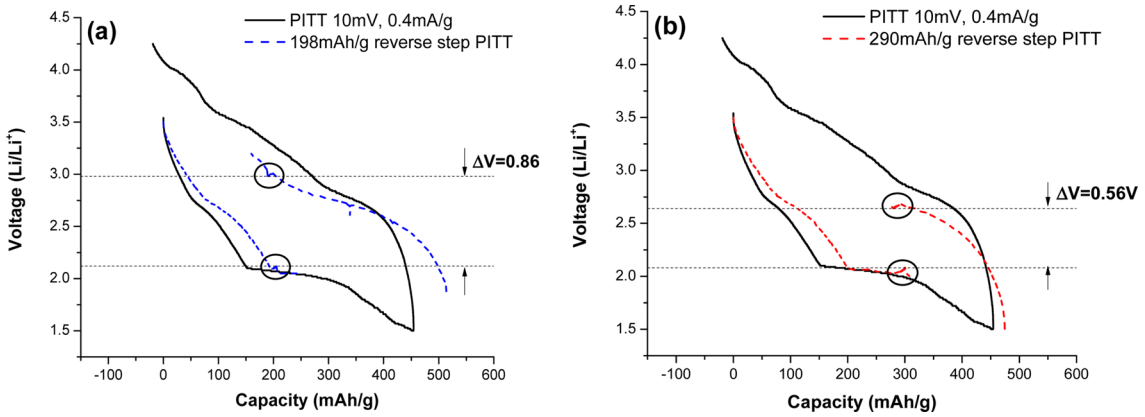

Figure 15. Reverse step PITT of $FeO_{0.67}F_{1.33}$ with its normal PITT overlay for capacities, the reverse step PITT portion are indicated with circle: (a) 198 mAh/g (x = 0.68) in the insertion region, (b) 290 mAh/g (x = 0.99) in the conversion region.

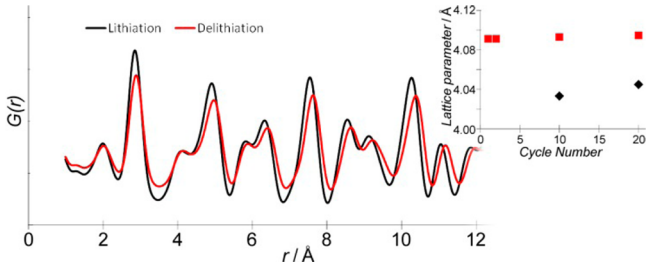

Figure 16. PDFs modeled for the LiF rocksalt components for the lithiated and delithiated electrodes showing the larger lattice parameter for this phase during delithiation. The refined lattice parameters for these phases are inset.

its composition, that is insertion/substitution of Li cations by larger Fe cations (likely Fe^{2+}), i.e., $Fe_xLi_{2-x}F_2$. Both the electrode composition and the lattice parameter of the rocksalt phase positively exclude the possibility that this is an unrelated rocksalt (e.g., $LiFeO_2$, $a \approx 4.3$ Å).

Two approaches were used to estimate the level of Fe substitution/insertion within the LiF: based on refinement of the structural model against the PDF, and based on the lattice expansion. In the PDF modeling, constraining the atomic displacement parameters for Li and F to the values refined for the lithiated state (and Fe to a reasonable value), x refined to 0.5 for $Fe_xLi_{2-x}F_2$. Although Vegard's law does not directly apply (as no rocksalt FeF_2 phase exists), assuming a linear relationship between the lattice volumes for pure rocksalt LiF and rutile-type FeF_2, the lattice dimensions refined for $Fe_xLi_{2-x}F_2$ correspond to $x \approx 0.4$. Although each approach has limitations, the similarity in the suggested levels of Fe substitution supports the existence of the Fe-substituted LiF rock salt phase $Fe_xLi_{2-x}F_2$.

Similar "normal" and expanded rocksalt-type LiF phases were observed upon lithiation and delithiation of FeF_3 suggesting that the Fe substituted $Fe_xLi_{2-x}F_2$ phase is also involved in the FeF_3 delithiation reaction as a precursor to the formation of its defective rutile formation described below. That the same lattice parameter is observed for $Fe_xLi_{2-x}F_2$ in both delithiated FeF_3 and delithiated FeF_2 suggests that this may represent the maximum substitution of Fe into LiF.

For the case of FeF_3, delithiation leads to the formation of a defective rutile structure. On the basis of our PITT results, composition changes are extremely small for each multiphasic reactions. Such phase evolution is supported by the multiple pathway defect rutile delithiation evolution proposed through first principles and also supported in part by characterization.[7,23,42] In particular, Yamakawa et al.[23] showed evidence of a sequential delithiation and formation of a rutile phase with lithium incorporation and iron oxidation state increasing with the state of charge.

FeOF presents interesting behavior upon lithiation. As opposed to the known conversion reaction of FeF_2 and FeF_3, we have a known reaction of (3)[13,26,28] representing P = 4. Similar to the delithiation reactions observed in the FeF_2 case, the lithiation reaction during the conversion reaction occurs in steps of minimal but not insignificant constant potential range. This may be related to nanometer oxygen gradients in the $FeO_{0.67}F_{1.33}$ phase utilized in this research or conversion phases of limited composition represented by (3). To have a constant potential of the four phase reaction in 3, i.e., F = 0, the number of components will have to be 4. Li, Fe, and F are required as independent components due to their mobility to form the LiF and Fe phases. Treating the rutile LiFeOF phase and the oxygen as the final fourth component would be acceptable as the diffusion of the oxygen is unlikely. This scenario leads to F = 0 and an invariant potential as a function of composition.

In contrast to scenario (3), scenario (4) consists of P = 3. In this structural evolution, one can treat the LiFeOF as more of a displacement vs. conversion material. Indeed, advanced characterization has yet to observe the conclusive presence of the LiF phase as a result of the conversion process and the phase has only been present under low potentials as a result from the decomposition of the rocksalt phase.[26,28] In this scenario, the rocksalt phase develops as a natural progression from the host rutile phase as lithium inserts into the rutile phase and displaces 0.5 Fe for every Li insertion. In this case, we can count the active components as 3; Li, Fe and the host compound transporting to the rocksalt phase. This scenario also leads to F = 0, a constant potential reaction.

In both scenarios the zero degree of freedom scenario suggest that the entire reaction should proceed as an invariant reaction. In contrast, the potential is observed to change with small degrees of constant potential with $\Delta x \ll 0.1$. This could be explained in the same manner as the delithiation reactions where in this case the rock salt phase has limited degrees of stable phase composition before the transformation to the next step.

$$Li^+ + LiFeOF \rightarrow LiF + 0.5Fe + LiFe_{0.5}O \quad (3)$$

dx.doi.org/10.1021/am500538b | ACS Appl. Mater. Interfaces 2014, 6, 10858−10869

$$Li^+ + LiFeOF \rightarrow 0.5Fe + Li_2Fe_{0.5}OF \quad (4)$$

If the above specified metal fluoride electrode reactions evolve a series of limited solubility multiphase reactions in near equilibrium requiring multimonth measurements, it is highly likely that most of these phases are not evolved during practical cycling rates. At such rates, the voltage induced by kinetic polarization will be such that near final phase compositions will be approached directly. This presents scenarios where reaction rates may dictate phase and morphology evolution, which then may influence ultimate electrochemical performance.

4.2. Hysteresis. The discussion above presents strong electrochemical evidence that a contrast in conversion reaction mechanism exists between the lithiation and delithiation reaction for the pure fluorides. This contrast in pathways manifests itself as an asymmetric intrinsic hysteresis. The contrast in mechanism between lithiation and delithiation also presents itself as a significant difference in the delta of the reaction potential between the lithiation and delithiation reaction relative to the thermodynamic potential of the reaction as defined by the Gibb's free energy of formation. FeF_2 is the only material which we have appropriate thermodynamic free energy of formation, a potential of 2.66 V vs Li/Li^+. For the lithiation reaction of 1, the hysteresis relative to the thermodynamic reaction potential is much greater than the multistep reaction of delithiation.

Ideally, the reaction path of an electrode material would be completely symmetric to induce minimal intrinsic hysteresis. Quantitative evidence for this can be found in the comparison of the 1.3 V hysteresis of the conversion regions of FeF_2 and FeF_3 vs. 0.7 V for $FeO_{0.67}F_{1.33}$ established under $C/1000$ reverse step PITT. The significant difference in observed hysteresis is consistent with the conversion reaction mechanisms discussed above. All the materials undergo multiple phase reactions with many changes in composition during delithiation. The pure fluorides present a single multiphase conversion reaction that goes to near completion during lithiation. Only the lithiation of $FeO_{0.67}F_{1.33}$ presents electrochemical evidence of a similar reaction mechanism during lithiation, as delithiation is consistent with a significant decrease in hysteresis.

4.3. Transport. The diffusion coefficients for all the conversion reactions were found to be in the range of $1-5 \times 10^{-18}$ cm^2/s. Although small, these diffusion values extracted over small composition perturbation techniques such as PITT and EIS are in excellent agreement with the times of diffusion typically observed during the macro length discharge of the fluorides. Specifically, it has been shown by Badway and later by Liao that reaction (particle) length scales must be <20 nm to achieve effective utilization of iron fluorides through the conversion reaction.[4,43] Applying the Einstein equation to the calculated diffusion coefficient of 4.0×10^{-18} cm^2/s derived by PITT for FeF_2 realizes a diffusion distance of 7.6 nm at a $C/20$ rate very consistent with a particle of 20 nm size with at least 2 sided diffusion access.

Most importantly, transport must be discussed in context to the conversion reaction. As opposed to a straight forward topotactic lithium insertion/deinsertion involving the mobility of Li^+ exclusively, the conversion reaction is dependent on the mobility of other species, namely Fe^{2+} or F^- as discussed in detail in the subject matter above. The mobility of these species is expected to be very slow but effective over small spatial dimensions. As such, they will exist as the limiting factor in phase front mobility and the effective diffusion coefficient, which should obviously be not attributed solely to the Li^+ ion.

5. CONCLUSIONS

High-resolution PITT of 10 mV steps to $C/1000$ current was found effective to isolate the true hysteresis of FeF_2, FeF_3, and $FeO_{0.67}F_{1.33}$ compounds relative to simple kinetically induced polarization. Reverse step PITT studies were used to remove effects induced by nucleation overpotential. Clear electrochemical evidence was seen for a significant asymmetry in lithiation/delithiation conversion reaction mechanisms for FeF_2 and FeF_3 while more symmetry was revealed for $FeO_{0.67}F_{1.33}$. This translated to similar hysteresis for FeF_2 and FeF_3 while $FeO_{0.67}F_{1.33}$ realized a significant reduction in hysteresis. This result strengthened the argument of reaction pathway asymmetry as the origin of kinetically unresolved hysteresis in conversion materials. Diffusion studies for the three materials realized similar low diffusion coefficients on the order of 1×10^{-18} cm^2/s, a value consistent with the required 20 nm to support a practical electrode reaction. High resolution PITT leads to new insights regarding the conversion reaction mechanisms. In one example, the reconversion process during delithiation reveal electrochemical and structural evidence of a $Fe_xLi_{2-2x}F_2$ rocksalt precursor forming prior to the reformation of FeF_2 rutile. The reaction was consistent with a multistep delithiation process observed within the PITT data.

AUTHOR INFORMATION

Corresponding Author

*E-mail: gamatucc@rci.rutgers.edu.

Notes

The authors declare no competing financial interest.

ACKNOWLEDGMENTS

This work is financially supported by the Northeastern Center for Chemical Energy Storage, an Energy Frontier Research Center, funded by the U.S. Department of Energy, Office of Basic Energy Sciences, under Award DE-SC0001294. Work done at Argonne and use of the Advanced Photon Source, an Office of Science User Facility operated for the U.S. Department of Energy Office of Science by Argonne National Laboratory, were supported by the U.S. Department of Energy under Contract DE-AC02-06CH11357. The authors thank G. Ceder, Stephen Garofalini, and A. Van der Ven for useful discussions.

REFERENCES

(1) Wang, F.; Robert, R.; Chernova, N. A.; Pereira, N.; Omenya, F.; Badway, F.; Hua, X.; Ruotolo, M.; Zhang, R.; Wu, L.; Volkov, V.; Su, D.; Key, B.; Whittingham, M. S.; Grey, C. P.; Amatucci, G. G.; Zhu, Y.; Graetz, J. Conversion Reaction Mechanisms in Lithium Ion Batteries: Study of the Binary Metal Fluoride Electrodes. *J. Am. Chem. Soc.* **2011**, *133*, 18828−18836.

(2) Parkinson, M. F.; Ko, J. K.; Halajko, A.; Sanghvi, S.; Amatucci, G. G. Effect of Vertically Structured Porosity on Electrochemical Performance of FeF_2 Films for Lithium Batteries. *Electrochim. Acta* **2014**, *125*, 71−82.

(3) Poizot, P.; Laruelle, S.; Grugeon, S.; Tarascon, J. M. Rationalization of the Low-Potential Reactivity of 3s-Metal-Based Inorganic Compounds toward Li. *J. Electrochem. Soc.* **2002**, *149* (9), A1212−A1217.

(4) Badway, F.; Cosandey, F.; Pereira, N.; Amatucci, G. G. Carbon Metal Fluoride Nanocomposites High-Capacity Reversible Metal

Fluoride Conversion Materials as Rechargeable Positive Electrodes for Li Batteries. *J. Electrochem. Soc.* **2003**, *150* (10), A1318−A1327.
(5) Badway, F.; Mansour, A. N.; Pereira, N.; Al-Sharab, J. F.; Cosandey, F.; Plitz, I.; Amatucci, G. G. Structure and Electrochemistry of Copper Fluoride Nanocomposites Utilizing Mixed Conducting Matrices. *Chem. Mater.* **2007**, *19* (17), 4129−4141.
(6) Bervas, M.; Badway, F.; Klein, L. C.; Amatucci, G. G. Bismuth Fluoride Nanocomposite as a Positive Electrode Material for Rechargeable Lithium Batteries. *Electrochem. Solid-State Lett.* **2005**, *8* (4), A179−A183.
(7) Doe, R. E.; Persson, K. A.; Meng, Y. S.; Ceder, G. First-Principles Investigation of the Li-Fe-F Phase Diagram and Equilibrium and Nonequilibrium Conversion Reactions of Iron Fluorides with Lithium. *Chem. Mater.* **2008**, *20*, 5274−5283.
(8) Dreyer, W.; Jamnik, J.; Guhlke, C.; Huth, R.; Moskon, J.; Gaberscek, M. The thermodynamic origin of hysteresis in insertion batteries. *Nat. Mater.* **2010**, *9*, 448−453.
(9) Moskon, J.; Jamnik, J.; Gaberscek, M. In depth discussion of selected phenomena associated with intrinsic bettery hysteresis: Battery electrode versus rubber balloons. *Solid State Ionics* **2013**, *238*, 24−29.
(10) Huggins, R. A.; Weppner, W. Determination of the Kinetic Parameters of Mized-Conducting Electrodes and Application to the System Li_3Sb. *J. Electrochem. Soc.* **1977**, *124* (10), 1569−1578.
(11) Wen, C. J.; Boukamp, B. A.; Huggins, R. A.; Weppner, W. Thermodynamic and Mass Transport Properties of "LiAl". *J. Electrochem. Soc.* **1979**, *126* (12), 2258−2266.
(12) Ho, C.; Raistrick, I. D.; Huggins, R. A. Application of A-C Techniques to the Study of Lithium Diffusion in Tungsten Trioxide Thin Films. *Electrochem. Sci. Technol.* **1980**, *127*, 343−350.
(13) Pereira, N.; Badway, F.; Wartelsky, M.; Gunn, S.; Amatucci, G. G. Iron Oxyfluorides as High Capacity Cathode Materials for Lithium Batteries. *J. Electrochem. Soc.* **2009**, *156*, A407−A416.
(14) Gozdz, A. S.; Schmutz, C.; Tarascon, J. M.; Warren, P. Polymetric Electrolytic Cell Seperator Membrane. U.S. Patent 5 418 091 May 23, 1995.
(15) Montella, C. Discussion of the potential step method for the determination of the diffusion coefficients of guest species in host materials Part I. Influence of charge transfer kinetics and ohmic potential drop. *J. Electroanal. Chem.* **2002**, *518*, 61−83.
(16) Vorotyntsev, M. A.; Levi, M. D.; Aurbach, D. Spatially limited diffusion coupled with ohmic potential drop and/or slow interfacial exchange: a new method to determine the diffusion time constant and external resistance from potential step (PITT) experiments. *J. Electroanal. Chem.* **2004**, *572*, 299−307.
(17) Chupas, P. J.; Qiu, X.; Hanson, J. C.; Lee, P. L.; Grey, C. P.; Billinge, S. J. L. Rapid-aquisition pair distribution function (RA-PDF) analysis. *J. Appl. Crystallogr.* **2003**, *36*, 1342−1347.
(18) Chupas, P. J.; Chapman, K. W.; Lee, P. L. Applications of an amorphous silicon-based area detector for high-resolution, high-sensitivity and fast time-resolved pair distribution function measurements. *J. Appl. Crystallogr.* **2007**, *40*, 463−470.
(19) Hammersley, A. P.; Svensson, S. O.; Hanfland, M.; Fitch, A. N.; Hausermann, D. Two-Dimensional Detector Software: From Real Detector to Idealised Image or Two-Theta Scan. *High Pressure Res.* **1996**, *14*, 235−248.
(20) Hammersley, A. P. *FIT2D: An Introduction and Overview*; ESRF internal report ESRF97HA02T ;European Synchrotron Research Foundation: Grenoble, France, 1997.
(21) Qiu, X.; Thompson, J. W.; Billinge, S. J. L. PDFgetX2: a GUI-driven program to obtain the pair distribution function from X-ray powder diffraction data. *J. Appl. Crystallogr.* **2004**, *37*, 678.
(22) Farrow, C. L.; Juhas, P.; Liu, J. W.; Bryndin, D.; Bozin, E. S.; Bloch, J.; Proffen, T.; Billinge, S. J. L. PDFfit2 and PDFgui: computer programs for studying nanostructure in crystals. *J. Phys.: Condens. Matter* **2007**, *19*, 33.
(23) Yamakawa, N.; Jiang, M.; Key, B.; Grey, C. P. Identifying the Local Structures Formed during Lithiation of the Conversion Materials, Iron Fluoride, in a Li Ion Battery: A Solid-State NMR, X-ray Diffraction, and Pair Distribution Function Analysis Study. *J. Am. Chem. Soc.* **2009**, *131*, 10525−10536.
(24) Xu, K.; Angell, C. A. High Anodic Stability of a New Electrolyte Solvent: Unsymmetric Noncyclic Aliphatic Sulfone. *J. Electrochem. Soc.* **1998**, *145* (4), L70−L72.
(25) Liu, P.; Vajo, J. J.; Wang, J. S.; Li, W.; Liu, J. Thermodynamics and Kinetics of the Li/FeF3 Reaction by Electrochemical Analysis. *J. Phys. Chem. C* **2012**, *116*, 6467−6473.
(26) Wiaderek, K. M.; Borkiewicz, O. J.; Castillo-Martinez, E.; Robert, R.; Pereira, N.; Amatucci, G. G.; Grey, C. P.; Chupas, P. J.; Chapman, K. W. Comprehensive Insights into the Structural and Chemical Changes in Mixed-Anion FeOF Electrodes by Using Operando PDF and NMR Spectroscopy. *J. Am. Chem. Soc.* **2013**, *135*, 4070−4078.
(27) Chevrier, V. L.; Hautier, G.; Ong, S. P.; Doe, R. E.; Ceder, G. First-principles study of iron oxyfluorides and lithiation of FeOF. *Phys. Rev. B:Condens. Matter Mater. Phys.* **2013**, *87*, 094118−0941-9.
(28) Cosandey, F.; Su, D.; Sina, M.; Pereira, N.; Amatucci, G. G. Fe valence determination and Li elemental distribution in Lithiated FeO0.7F1.3/C nanocomposite battery materials by electron energy loss spectroscopy (EELS). *Micron* **2012**, *43*, 22−29.
(29) Sougrati, M. T.; Jumas, J. C.; Pereira, N.; Amatucci, G. G. unpublished work. 2013.
(30) Levi, M. D.; Gamolsy, K.; Aurbach, D.; Heider, U.; Oesten, R. Determination of the Li ion chemical diffusion coefficient for the topotactic solid-state reactions occuring via a two-phase or single-phase solid solution pathway. *J. Electroanal. Chem.* **1999**, *477*, 32−40.
(31) Levi, M. D.; Markevich, E.; Aurbach, D. Comparison between Cottrell diffusion and moving boundary models for determination of the chemical diffusion coefficients in ion-insertion electrodes. *Electrochim. Acta* **2005**, *51*, 98−110.
(32) Decker, F.; Donsanti, F.; Salvi, A. M.; Ibris, N.; Castle, J. E.; Martin, F.; Alamarguy, D.; Vuk, A. S.; Orel, B.; Lourenco, A. Li^+ Distribution into V_2O_5 Films resulting from Electrochemical Intercalation Reactions. *J. Braz. Chem. Soc.* **2008**, *19*, 667−671.
(33) Dell'Era, A.; Pasquali, M. Comparison between different ways to determine diffusion coefficient and by solving Fick's equation for spherical coordinates. *J. Solid State Electrochem.* **2009**, *13*, 849−859.
(34) Fell, C. R.; Carroll, K. J.; Chi, M.; Meng, Y. S. Sythesis-Structure-Property Relations in Layered, "Li-excess" Oxides Electrode Materials $Li[Li_{1/3-2x/3}Ni_xMn_{2/3-x/3}]O_2$ (x = 1/3, 1/4, and 1/5). *J. Electrochem. Soc.* **2010**, *157*, A1201−A1211.
(35) Levi, M. D.; Salitra, G.; Markovsky, B.; Teller, H.; Aurbach, D.; Heider, U.; Heider, L. Solid-State Electrochemical Kinetics of Li-Ion Intercalation into $Li_{1-x}CoO_2$: Simultaneous Application of Electroanalytical Techniques SSCV, PITT, and EIS. *J. Electrochem. Soc.* **1999**, *146*, 1279−1289.
(36) Rho, Y.; Kanamura, K. Li^+-Ion Diffusion in $LiCoO_2$ Thin Film Prepared by the Poly(vinylpyrrolidone) Sol−Gel Method. *J. Electrochem. Soc.* **2004**, *151*, A1406−A1411.
(37) Delacourt, C.; Ati, M.; Tarascon, J. M. Measurement of Lithium Diffusion Coefficient in Li_yFeSO_4F. *J. Electrochem. Soc.* **2011**, *158*, A741−A749.
(38) Li, J.; Xiao, X.; Yang, F.; Verbrugge, M. W.; Cheng, Y. Potentiostatic Intermittent Titration Technique for Electrodes Governed by Diffusion and Interfacial Reaction. *J. Phys. Chem. C* **2012**, *116*, 1472−1478.
(39) Huggins, R. A. Principles determining the potentials and capacities of electrochemical cells. *NATO Sci. Ser., III* **200**, *85*, 21−46.
(40) Huggins, R. A. Reference electrodes and the Gibbs phase rule. *Solid State Ionics* **2000**, *136-137*, 1321−1328.
(41) Huggins, R. A. The relation between the Gibbs phase rule and reference electrodes. *Ionics* **1998**, *4*, 129−140.
(42) Badway, F.; Pereira, N.; Cosandey, F.; Amatucci, G. G. Cabon-Metal Fluoride Nanocomposites Structure and Electrochemistry of FeF_3:C. *J. Electrochem. Soc.* **2003**, *150*, A1209−A1218.
(43) Liao, P.; Li, J.; Dahn, J. R. Lithium Intercalation in $LiFe_2F_6$ and $LiMgFeF_6$ Disordered Trirutile-Type Phases. *J. Electrochem. Soc.* **2010**, *157*, A355−A361.